Propagation of lower hybrid resonance cones in tokamaks

P. M. Bellan
California Institute of Technology, Pasadena, California 91125

(Received 18 May 1982; accepted 9 November 1982)

The trajectory of the lower hybrid resonance cone surface is calculated for propagation in the helical magnetic field of a tokamak. The surface is found to be a deformed cone, having symmetry axis following the magnetic field helicity. By superimposing cone fields excited by adjacent, poloidally separated point sources, the field excited by a source of finite poloidal extend is deduced. For sources having large poloidal extent, the superimposed cones destructively interfere everywhere except in a small region of constructive reinforcement which is located towards the plasma center; sources having small poloidal extent excite an individual resonance cone, which extends from near the plasma center all the way to the wall. Numerical calculations are presented for Verasator, Alcator-A and -C, JFT-2, and PLT tokamak parameters.

I. INTRODUCTION

The propagation of lower hybrid waves in tokamaks is not completely understood, because (i) the twisted magnetic geometry of tokamaks complicates theoretical models, and (ii) experimental measurements of wave propagation in high temperature tokamaks are extremely difficult. (In contrast, there is excellent understanding[1–4] of lower hybrid propagation in low temperature plasmas having straight magnetic field lines, because both theoretical models and experimental measurements are straightforward.)

An essential feature of lower hybrid wave propagation is that the geometric shape of the excited field depends critically on the antenna geometry. In particular, an infinite extent antenna (phased to excite a single Fourier mode) excites a plane wave extending over the entire volume, whereas a point source antenna excites a highly localized field called a resonance cone. The relation between the resonance cone field and the infinite source field is essentially the relation between a delta function and its Fourier transform. Sources of finite extent excite fields having properties of both the point and the infinite extent sources.

Ray tracing codes predicting the trajectory of a single plane wave ray in a tokamak exist[5,6] and give valuable insights on lower hybrid wave propagation in tokamaks. However, the single plane wave model used in these codes is not really appropriate for describing the lower hybrid wave field excited by a finite size, localized antenna, such as the "grill" antenna[7] used in tokamaks. This is because the single plane wave ray corresponds to the field excited by a source of infinite, rather than finite extent. To find the field excited by a source of finite extent, one can proceed two ways: (i) one can Fourier decompose the finite source into a sum of plane waves, calculate the propagation of each plane wave, and then superimpose the results; or (ii) one can split the finite source into a group of adjacent point sources, calculate the resonance cone excited by each point source, and then superimpose the results. Method (ii) is somewhat more intuitive, and will be used here. The procedure thus involves calculation of the behavior of resonance cones in tokamak geometry. In straight field line geometries (where cones have been studied in great detail) it has been shown that the resonance cone has apex at the antenna, axis along the magnetic field, and cone angle $\theta_c = \tan^{-1}(-K_\perp/K_\parallel)^{1/2}$, where $K_\perp$ and $K_\parallel$ are, respectively, the plasma perpendicular and parallel dielectric tensor elements. One might surmise that, for a cone propagating in the helical magnetic geometry of a tokamak, the cone axis will also be helical, so that the resultant deformed cone would look something like a ram's horn.

In this paper we present a combined analytic and numerical calculation of these twisted cones. To make the analysis tractable, the electrostatic and cold plasma approximations are employed; electromagnetic[8] and thermal effects[1,2,9] are neglected. Phasing of the source elements,[10] and the finite extent[10] of the source will be considered by superimposing fields excited by adjacent point sources. Scattering of the lower hybrid wave by density fluctuations[11–15] (which can be a dominant process if the density fluctuations are sufficiently strong) will not be considered here.

The paper is organized as follows. In Sec. II we give the derivation of the cone ray tracing equations for straight cylindrical tokamaks having arbitrary magnetic field helicity. To integrate these equations, the initial functional dependence of the cone rays is required. This dependence is calculated in Sec. III using coordinate system transformations to express a tilted cone surface in laboratory coordinates. In Sec. IV we give the results of numerical integrations of the cone ray equations, and discuss the superposition of cones excited by adjacent point sources (the representation of a finite extent source). In Sec. V a brief summary is given.

II. CONE RAY TRACING EQUATIONS

The electrostatic wave equation is

$$\frac{\partial}{\partial \mathbf{x}_\perp}\cdot\mathbf{K}\cdot\frac{\partial\varphi}{\partial\mathbf{x}_\perp}+\frac{\partial}{\partial\mathbf{x}_\parallel}\cdot\mathbf{K}\cdot\frac{\partial\varphi}{\partial\mathbf{x}_\parallel}=0, \tag{1}$$

where $\perp$ and $\parallel$ are relative to the confining magnetic field $\mathbf{B}=B_\theta(r,\theta)\hat{\theta}+B_z(r,\theta)\hat{z}$. Defining $\eta=B_\theta/B_z$, the magnetic field unit vector becomes $\hat{B}=(\eta\hat{\theta}+\hat{z})/(1+\eta^2)^{1/2}$ and the derivatives parallel and perpendicular to $\mathbf{B}$ become

 0031-9171/83/030741-06$01.90 © 1983 American Institute of Physics

Downloaded 13 Dec 2007 to 131.215.225.196. Redistribution subject to AIP license or copyright; see http://pof.aip.org/pof/copyright.jsp

$$\frac{\partial}{\partial \mathbf{x}_\parallel} = \frac{\hat{B}}{(1+\eta^2)^{1/2}}\left(\frac{\eta}{r}\frac{\partial}{\partial\theta} + \frac{\partial}{\partial z}\right),$$

$$\frac{\partial}{\partial \mathbf{x}_\perp} = \hat{r}\frac{\partial}{\partial r} + \frac{\hat{\theta}}{1+\eta^2}\left(\frac{1}{r}\frac{\partial}{\partial\theta} - \eta\frac{\partial}{\partial z}\right) + \frac{\hat{z}}{1+\eta^2}\left(\eta^2\frac{\partial}{\partial z} - \frac{\eta}{r}\frac{\partial}{\partial\theta}\right). \quad (2)$$

To solve Eq.(1), the potential is assumed to be a distorted resonance cone of the form

$$\varphi = \Phi[z - af(r/a,\theta)]; \quad (3)$$

here a is the tokamak minor radius, and curves of constant f (to be determined) give projections of the resonance cone on the r,θ plane. The cold electrostatic resonance cone has a delta function dependence and so is infinitely sharp, i.e., it has a characteristic scale length of zero. However, when the thermal, electromagnetic, and toroidal extent of the exciting antenna are taken into account, the resonance cone is found to have a finite amplitude and correspondingly, a nonzero scale length. However, this scale length is still typically much smaller than the scale length of plasma equilibrium, quantities (e.g., density, magnetic field, η). For typical tokamak parameters the cone versus equilibrium scale lengths compare as 10^{-2}–10^{-1} cm versus 10–100 cm, respectively. Thus, derivatives of φ involving resonance cone scale lengths will be much larger than those involving equilibrium scale lengths, i.e., $a^2\Phi'' \gg a\Phi' \gg \Phi$. Hence, to lowest order, the terms involving Φ' and Φ, may be dropped when Eq. (3) is substituted into Eq. (1). Thus, solving Eq. (1) amounts to setting the coefficient of Φ'' to zero (this is similar to the Eikonal approximation used for plane wave ray tracing). The coefficient of Φ'' is

$$D = [(1+\eta^2)f_\xi^2 + (f_\theta/\xi + \eta)^2]K_\perp + (1 - nf_\theta/\xi)^2 K_\parallel \quad (4)$$

where $\xi = r/a$. This expression for D is exact—no assumption concerning smallness of the helicity factor η has been made. In a manner similar to plane wave ray tracing, here a *cone ray trajectory* is defined as the locus on which $D = 0$ holds; i.e., along a cone ray trajectory

$$\delta D = \left(\frac{\partial D}{\partial f_\xi}\frac{\partial f_\xi}{\partial\tau} + \frac{\partial D}{\partial\xi}\frac{\partial\xi}{\partial\tau} + \frac{\partial D}{\partial f_\theta}\frac{\partial f_\theta}{\partial\tau} + \frac{\partial D}{\partial\theta}\frac{\partial\theta}{\partial\tau}\right)d\tau = 0,$$

where τ is the distance along the ray path. This requirement is satisfied by setting

$$\frac{\partial\xi}{\partial\tau} = \frac{\partial D}{\partial f_\xi}, \quad \frac{\partial f_\xi}{\partial\tau} = -\frac{\partial D}{\partial\xi},$$

$$\frac{\partial\theta}{\partial\tau} = \frac{\partial D}{\partial f_\theta}, \quad \frac{\partial f_\theta}{\partial\tau} = -\frac{\partial D}{\partial\theta}. \quad (5)$$

The cone projection on the ξ,θ plane, i.e., the surface $f(\xi,\theta) = \text{const}$ is what is desired. As Eqs. (5) stand, they do not give this surface because $df/d\tau$ is not the same on each of the cone rays described by Eqs. (5). In other words, the tips of the rays at a particular value of τ do *not* correspond to a surface of constant f. This difficulty may be removed by replacing τ with a "stretched" path parameter, τ', defined so that all the ray tips correspond to the same value of f. By considering the incremental change in f along a ray,

$$df = \delta\mathbf{x}\cdot\nabla f = \left(\frac{\partial\xi}{\partial\tau}f_\xi + \frac{\partial\theta}{\partial\tau}f_\theta\right)d\tau$$

where $\delta\mathbf{x}$ is the path increment along the ray, it is seen that a suitable definition for τ' is

$$d\tau' = \left(\frac{\partial\xi}{\partial\tau}f_\xi + \frac{\partial\theta}{\partial\tau}f_\theta\right)d\tau = \left(f_\xi\frac{\partial D}{\partial f_\xi} + f_\theta\frac{\partial D}{\partial f_\theta}\right)d\tau.$$

Since $d/d\tau = g^{-1}d/d\tau'$, where $g = [f_\xi(\partial D/\partial f_\xi) + f_\theta(\partial D/\partial f_\theta)]^{-1}$, Eq. (5) becomes

$$\frac{\partial\xi}{\partial\tau'} = g\frac{\partial D}{\partial f_\xi}, \quad \frac{\partial f_\xi}{\partial\tau'} = -g\frac{\partial D}{\partial\xi},$$

$$\frac{\partial\theta}{\partial\tau'} = g\frac{\partial D}{\partial f_\theta}, \quad \frac{\partial f_\theta}{\partial\tau'} = -g\frac{\partial D}{\partial\theta}. \quad (6)$$

III. INITIAL CONDITIONS

Equation (6) is to be numerically integrated for each cone ray; the locus of ray tips at a particular value of τ' gives the projection of the cone onto the ξ,θ plane. To start the integration it is necessary to know the initial values of f_ξ and f_θ of each cone ray at the source position ξ_s,θ_s (the z axis origin is chosen so that $z_s = 0$). Since the cone rays described by Eqs. (6) are loci of the surface $D = 0$, it is critical that the initial values of f_ξ and f_θ, upon substitution into Eq. (4), satisfy $D = 0$ as accurately as possible. Hence, it is important to calculate the initial values of f_ξ and f_θ to a very high degree of accuracy.

Such very accurate initial values may be found as follows. In the immediate neighborhood of the source the field is the simple resonance cone[1-3]

$$z'_{\text{loc}} = \alpha r'_{\text{loc}}. \quad (7)$$

Here $z'_{\text{loc}}, r'_{\text{loc}}$ are the axial and radial components of a cylindrical coordinate system in which the origin is at the source and the z_{loc} axis lies along the magnetic field passing through the source, while $\alpha = (-K_\parallel/K_\perp)^{1/2}$, where $K_\parallel$ and $K_\perp$ are evaluated in the immediate neighborhood of the source. The procedure for determining the initial conditions will be: (i) express Eq. (7) in the lab coordinate system ξ, θ, z; (ii) rearrange this expression to have the same form as the argument of Φ in Eq. (3); (iii) identify f from the rearranged expression; and (iv) calculate the initial values of f_ξ and f_θ by taking derivatives of f.

The geometry of the local-to-lab coordinate transformation is shown in Fig. 1(a). From Fig. 1(a) it can be seen that the relation between the lab coordinate system ξ, θ, z and a Cartesian coordinate system z_{loc}, y_{loc}, z_{loc} with local z axis parallel to the lab z axis and origin at the source, is that *at the source*

$$\hat{x}_{\text{loc}} = \hat{r}, \quad \hat{y}_{\text{loc}} = \hat{\theta}, \quad \hat{z}_{\text{loc}} = \hat{z}.$$

Now, as shown in Fig. 1(b), by looking down the $\hat{x}_{\text{lox}}$ (or equivalently $\hat{r}$ axis), the relation between the primed (z axis parallel to the local magnetic field) and the unprimed (z axis

Downloaded 13 Dec 2007 to 131.215.225.196. Redistribution subject to AIP license or copyright; see http://pof.aip.org/pof/copyright.jsp

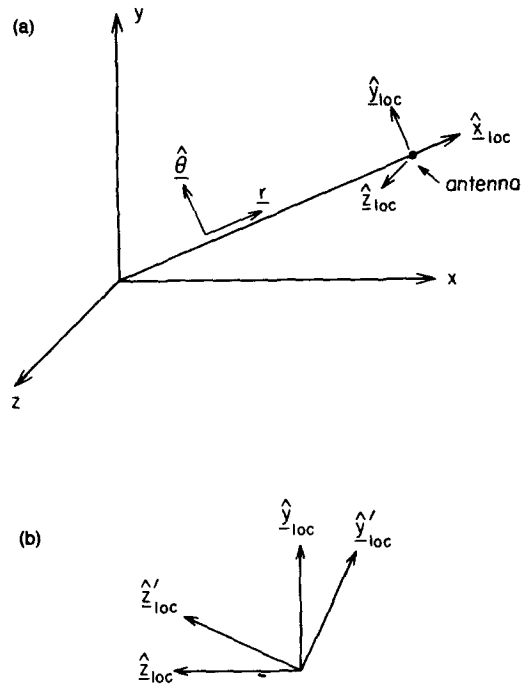

FIG. 1. Geometry of coordinate transformations: (a) local-to-lab coordinate transformation; (b) relation between the primed (z axis parallel to local magnetic field) and unprimed (z axis parallel to lab z axis) unit vectors.

parallel to lab z axis) z unit vectors is seen to be

$$\hat{z}'_{loc} = \hat{B} = (\hat{z}_{loc} + \eta\hat{\theta})/(1+\eta^2)^{1/2}.$$

Because $\hat{y}'_{loc}$ is orthogonal to $\hat{z}'_{loc}$,

$$\hat{y}'_{loc} = (\hat{\theta} - \eta\hat{z}_{loc})/(1+\eta^2)^{1/2}.$$

In terms of the lab coordinates these relations become

$$\hat{x}'_{loc} = \hat{r},$$
$$\hat{y}'_{loc} = (\hat{\theta} - \eta\hat{z})/(1+\eta^2)^{1/2},$$
$$\hat{z}'_{loc} = (\hat{z} + \eta\hat{\theta})/(1+\eta^2)^{1/2},$$

a set of mutually orthogonal unit vectors.

Vectors in the local and lab coordinate systems are related by

$$\mathbf{r}_{loc} = \mathbf{r} - r_s$$

where r_s is the source location. Components in the local primed coordinate system are given by $x'_{loc} = \mathbf{r}_{loc}\cdot\hat{x}'_{loc}$ etc., so that the local primed to lab conversion is given by

$$x'_{loc} = (\mathbf{r} - r_s)\cdot\hat{r} = r - r_s\cos(\theta - \theta_s),$$
$$y'_{loc} = (\mathbf{r} - r_s)\cdot\frac{(\hat{\theta} - \eta\hat{z})}{(1+\eta^2)^{1/2}} = \frac{r_s\sin(\theta-\theta_s) - \eta z}{(1+\eta^2)^{1/2}}, \tag{8}$$
$$z'_{loc} = (\mathbf{r} - r_s)\cdot\frac{(\hat{z} + \eta\hat{\theta})}{(1+\eta^2)^{1/2}} = \frac{z + \eta r_s\sin(\theta-\theta_s)}{(1+\eta^2)^{1/2}}.$$

Noting $r'_{loc} = (x'^2_{loc} + y'^2_{loc})^{1/2}$ and using Eq. (8) to substitute for the primed local coordinates in Eq. (7) gives

$$\frac{z + \eta r_s\sin\delta}{(1+\eta^2)^{1/2}} = \alpha\left[(r - r_s\cos\delta)^2 + \left(\frac{r_s\sin\delta - \eta z}{(1+\eta^2)^{1/2}}\right)^2\right]^{1/2}, \tag{9}$$

where $\delta = \theta - \theta_s$.

Squaring Eq. (9) gives a quadratic in z the solution of which is

$$z = (-(1+\alpha^2)\eta r_s\sin\delta + \{[(1+\alpha^2)\eta r_s\sin\delta]^2 - (1-\eta^2\alpha^2)[-\alpha^2(1+\eta^2)(r - r_s\cos\delta)^2 + (\eta^2-\alpha^2)r_s^2\sin^2\delta]\}^{1/2})(1-\eta^2\alpha^2)^{-1}. \tag{10}$$

The root with positive square root has been selected because it is one that corresponds to Eq. (7) when $\eta\to 0$.

On the cone surface the argument of Φ is zero, i.e., $z = af(\xi,\theta)$. Since Eq. (10) gives the cone surface near the source, f can be identified from Eq. (10) as being

$$f(\xi,\theta) = (-(1+\alpha^2)\eta\xi_s\sin\delta + \{[(1+\alpha^2)\eta\xi_s\sin\delta]^2 - (1-\eta^2\alpha^2)[-\alpha^2(1+\eta^2)(\xi - \xi_s\cos\delta)^2 + (\eta^2-\alpha^2)\xi_s^2\sin^2\delta]\}^{1/2})(1-\eta^2\alpha^2)^{-1}. \tag{11}$$

The desired initial condition for each cone ray is then found from the derivatives of Eq. (11),

$$f_\xi = \frac{\alpha^2(1+\eta^2)(\xi - \xi_s\cos\delta)}{\{[(1+\alpha^2)\eta\xi_s\sin\delta]^2 - (1-\eta^2\alpha^2)[-\alpha^2(1+\eta^2)(\xi-\xi_s\cos\delta)^2 + (\eta^2-\alpha^2)\xi_s^2\sin^2\delta]\}^{1/2}},$$
$$f_\theta = \frac{(1+\alpha^2)\eta\xi_s\cos\delta}{1-\eta^2\alpha^2} + \frac{[(1+\alpha^2)\eta\xi_s]^2\sin\delta\cos\delta + (1-\eta^2\alpha^2)[(\alpha^2-\eta^2)\xi_s^2\sin\delta\cos\delta + \alpha^2(1+\eta^2)(\xi - \xi_s\cos\delta)\xi_s\sin\delta]}{(1-\eta^2\alpha^2)\{[(1+\alpha^2)\eta\xi_s\sin\delta]^2 - (1-\eta^2\alpha^2)[-\alpha^2(1+\eta^2)(\xi-\xi_s\cos\delta)^2 + (\eta^2-\alpha^2)\xi_s^2\sin^2\delta]\}^{1/2}}. \tag{12}$$

As mentioned earlier, the source excites a number of rays, the sum of which make up the cone surface. Thus, Eq. (10) does not describe a unique ray, but rather a set of rays. Each ray may be labeled according to its initial value of δ. To find $\xi(\delta)$, Eq. (9) is squared again and the quadratic for ξ is solved, where now $z = af$ is considered as a constant, giving

$$\xi(\delta) = \xi_s\cos\delta \pm \left(\frac{(f + \eta\xi_s\sin\delta)^2}{\alpha^2(1+\eta^2)} - \frac{(\xi_s\sin\delta - \eta f)^2}{(1+\eta^2)}\right)^{1/2}. \tag{13}$$

The range of δ over which rays exist is determined by the range of $\sin\delta$ for which the square root in Eq. (13) is real; thus, the maximum and minimum allowed values of δ occur when the square root argument is zero; i.e., when

$$\sin\delta_{max,min} = \frac{f}{\xi_s}\left(\frac{-\eta(1+\alpha^2) \pm [\eta^2(1+\alpha^2)^2 - (\eta^2-\alpha^2)(1-\eta^2\alpha^2)]^{1/2}}{\eta^2-\alpha^2}\right). \tag{14}$$

Downloaded 13 Dec 2007 to 131.215.225.196. Redistribution subject to AIP license or copyright; see http://pof.aip.org/pof/copyright.jsp

Thus, for $\delta_{\min} < \delta < \delta_{\max}$ the initial cone ray tips are given by Eq. (13).

Hence, to start the cone ray integration, f is chosen to be some small number and δ is varied over its allowed range, $\delta_{\min} < \delta < \delta_{\max}$. Each value of δ specifies an initial cone ray, with its specific initial $\xi(\delta)$, $f_\xi(\xi(\delta),\delta)$, and $f_\theta(\xi(\delta),\delta)$. For each of these rays a trajectory is calculated using Eqs. (6). To obtain the projection of the cone surface on the ξ,θ plane the locus of ray tips is plotted for $\tau' = f$.

IV. CONE SURFACES AND FIELDS EXCITED BY FINITE EXTENT SOURCES

A. Numerically integrated cone surfaces

The explicit forms of the derivatives of D are given in the Appendix. For the numerical results which follow, the density and toroidal magnetic field profiles are related to their values n_{axis}, B_{axis} at the magnetic axis by:

$$n = n_{\text{axis}}(1 - \xi^2),$$

$$B_z = \frac{B_{\text{axis}}}{[1 + (r/R)\cos\theta]} = \frac{B_{\text{axis}}}{(1 + \epsilon\xi\cos\theta)},$$

where $\epsilon = a/R$ is the inverse aspect ratio. The poloidal field is given by

$$B_\theta = rB_z/Rq = \epsilon\xi B_z/q,$$

where the safety factor q is given by the standard parameterization[16]

$$q = q_{\text{axis}}\left[1 + \left(\frac{r}{r_0}\right)^{2\lambda}\right]^{1/\lambda} = q_{\text{axis}}\left[1 + \left(\frac{\xi}{r_0/\alpha}\right)^{2\lambda}\right]^{1/\lambda}$$

and r_0 and λ are measures of the current channel width. From these relations it is seen that

$$\eta = \epsilon\xi/q(\xi).$$

Equations (6) were numerically integrated on an LSI-11/23 minicomputer for a set of 21 cone rays using the initial conditions specified by Eqs. (12)–(14); a value of $f = 10^{-5}$ was used for Eq. (14). The accuracy of the computation was continuously checked by evaluating the relative error in the condition $D = 0$ at each step in the integration for each ray. Here, relative means (computed D)/(largest term of the terms making up D). Because of the accuracy of the initial conditions, this relative error was very small, typically 10^{-6}–10^{-3}. Figure 2 shows plots of the computed cone projections (i.e., the constant f surfaces given by the loci of the tips of the cone rays) for typical Alcator-C[17] parameters (toroidal separation between adjacent cone projections is one minor radius). The ram's horn shape of the twisted cone surface is clearly evident. Significant features of this plot are:

(i) The cone spreads out in the direction perpendicular to its propagation direction, so that its energy density decreases.

(ii) Once the cone has penetrated moderately into the plasma the phase velocity direction of fine structure wiggles caused by thermal or electromagnetic effects depends strongly on the location of the wiggles on the cone. On the innermost, central, and outermost parts of the cone respectively, the fine structure phase velocity point radially inward, and radially outward.

(iii) The cone undergoes a form of spatial dispersion, or "skidding," because the inner part of the cone propagates at a different angular rate (due mainly to the higher density near the magnetic axis) than the outer part of the cone.

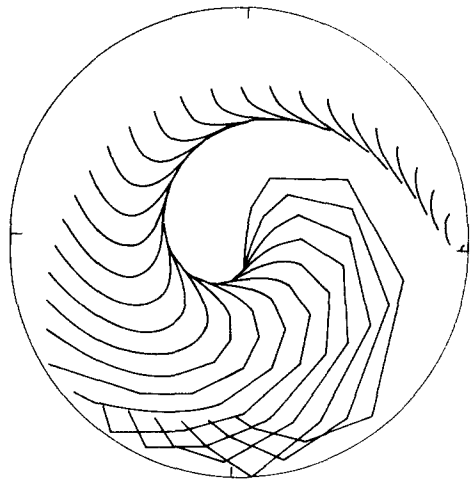

FIG. 2. Projections of cone surface on the minor cross section for toroidal positions separated by one minor radius; Alcator-C parameters used: $B_z = 82$ kG, $n_{\text{axis}} = 5\times10^{15}$ cm^{-3}, major radius $R = 64$ cm, minor radius $a = 17$ cm, $r_0 = 9.35$ cm and $\lambda = 2$, safety factor $q = 1$ at magnetic axis and $q = 3.4$ at wall, $f = 4.6$ GHz, deuterium gas, source located on midplane at minor radius of 16.7 cm.

(iv) The outer part of the cone is continuously moving radially outward (while the inner part moves inward). The outer part starts scraping against the wall; as each segment of cone touches the wall it reflects.

Thus, the wave energy is quite spread out and the wave-vector direction of the structure inside the cone envelope varies considerably.

Figures 3(a)–(d) show cone projection plots for typical Versator[18], Alcator-A[19], JFT-2[20], and PLT[21] parameters (in these figures the separation between projections is one quarter of the toroidal circumference). The same qualitative behavior as Fig. 2 is evident.

B. Fields excited by finite extent sources

This analysis has been done for a print source. In actual fact, the grill antennas typically used for excitation of lower hybrid waves have both finite toroidal and poloidal extent. The finite toroidal extent (and the passing of the antenna) will determine the structure of the fine structure of cone, as described in Refs. 4 and 9.

The effect of finite poloidal extent is demonstrated in Fig. 4(a) where cones excited by point sources at the midplane (solid line), and slightly above (dotted line) and below (dashed line) the midplane are shown. To understand how these cones superimpose, it should be remembered that the cones have a fine structure due to a combination of electromagnetic and thermal effects neglected in the cold electrostatic approximation, and also due to the toroidal phasing of the antenna. As shown schematically in Figs. 4(b) and (c) superimposed separated cones may or may not destructively interfere, depending on how the width of the region of overlap compares to the fine structure wavelength. In Fig. 4(b) the region of overlap is narrow, giving little destructive interference, and so the net superimposed field looks like the indi-

Downloaded 13 Dec 2007 to 131.215.225.196. Redistribution subject to AIP license or copyright; see http://pof.aip.org/pof/copyright.jsp

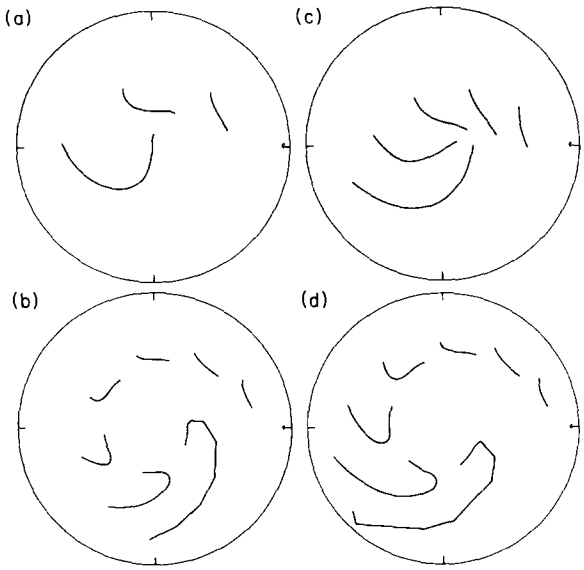

FIG. 3. Same as Fig. 2 except toroidal positions separated by one quarter toroidal circumference, and machine parameters are (a) Versator ($B_z = 8$ kG, $n_{axis} = 4\times10^{12}$ cm^{-3}, $R = 40$ cm, $a = 13$ cm, $r_0 = 5.2$ cm, $q = 1$ at magnetic axis and $q = 6.3$ at wall, $f = 0.8$ GHz, deuterium gas, source at minor radius of 12.8 cm); (b) Alcator-A ($B_z = 60$ kG, $n_{axis} = 2\times10^{14}$ cm^{-3}, $R = 54$ cm, $a = 12.7$ cm, $r_0 = 5.0$ cm, $q = 1$ at magnetic axis and $q = 6.5$ at wall, $f = 2.5$ GHz, deuterium gas, source at minor radius of 12.5 cm); (c) JFT-2 ($B_z = 14$ kG, $n_{axis} = 6\times10^{12}$ cm^{-3}, $R = 90$ cm, $a = 25$ cm, $r_0 = 10$ cm, $q = 2$ at magnetic axis and $q = 12.6$ at wall, $f = 0.75$ GHz, deuterium gas, source at minor radius of 24.5 cm); (d) PLT ($B_z = 35$ kG, $n_{axis} = 2\times10^{13}$ cm^{-3}, $R = 130$ cm, $a = 45$ cm, $r_0 = 18$ cm, $q = 1$ at magnetic axis and $q = 6.3$ at wall, $f = 0.8$ GHz, deuterium gas, source at minor radius of 44.1 cm).

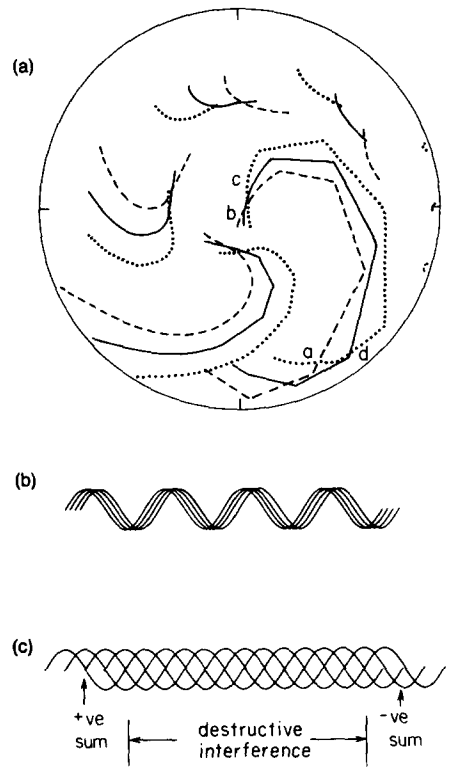

FIG. 4. Effect of finite poloidal extent of source: (a) Cones excited by poloidally separated sources, dotted line corresponds to source 5 cm above midplane, dashed to 5 cm below, solid to source on midplane. Alcator-C parameters, cone projections are for increments of quarter major circumference, and all sources at 16.7 cm minor radius; (b) overlap of cone fine structure over narrow region gives little phase cancellation; (c) overlap over wide region gives phase cancellation except at boundaries of region (positive and negative sums).

vidual resonance cones. In Fig. 4(c) the region of overlap is wide and so there is destructive interference except at the boundaries of the region of overlap [positive and negative sums in Fig. 4(c)].

From Fig. 4(a) it is seen that, the region of narrow overlap is a short line [e.g., line bc in Fig. 4(a)] near the plasma center, while the region of wide overlap contains the rest of the resonance cones (e.g., region between ab and dc). Hence, if the source has a large poloidal extent most of the field will be located at the region of narrow overlap (line bc), with a somewhat weaker field appearing at the boundaries of the region of wide overlap (lines ab and dc). As the poloidal extent of the source is reduced, the region of narrow overlap will increase, until it becomes the entire cone surface (i.e., lines ab and dc will coalesce).

For practical antennas, the poloidal extent is typically large enough so that the cone surfaces ab and dc in Fig. 4(a) are separated by much more than the fine structure period. Hence, most of the energy will be concentrated in the small region where there is narrow overlap [i.e., line bc in Fig. 4(a)]. In contrast to the behavior of individual resonance cones, the extent of this region of constructive interference *decreases* as the waves penetrate into the plasma. Thus, in agreement with intuition, sources of small poloidal extent generate divergent fields (the cones), whereas fields of large poloidal extent generate convergent fields (the small region of constructive interference).

V. SUMMARY

The geometric shape of the resonance cones in the helical fields of tokamaks has been calculated using an Eikonal-like technique, and the resonance cone surface has been shown to look like a ram's horn. For sources of finite poloidal extent, superposition of these cone surfaces results in phase cancellation except at a small region near the plasma center. As the poloidal extent of the source is reduced the field spreads out until it reverts to being the resonance cone surface.

ACKNOWLEDGMENTS

This work was supported by National Science Foundation Grant No. ECS-8113533. The author is an Alfred P. Sloan Foundation Fellow.

APPENDIX: D DERIVATIVES AND THE PLASMA DIELECTRIC

The explicit derivatives of D used for the integration of Eq. (6) are

Downloaded 13 Dec 2007 to 131.215.225.196. Redistribution subject to AIP license or copyright; see http://pof.aip.org/pof/copyright.jsp

$$\frac{\partial D}{\partial f_\xi} = 2(1+\eta^2) f_\xi K_\perp ,$$

$$\frac{\partial D}{\partial f_\theta} = \frac{2}{\xi}\left[\left(\frac{f_\theta}{\xi}+\eta\right)K_\perp - \left(1-\frac{\eta f_\theta}{\xi}\right)\eta K_\parallel\right],$$

$$\frac{\partial D}{\partial \xi} = \left[(1+\eta^2)f_\xi^2 + \left(\frac{f_\theta}{\xi}+\eta\right)^2\right]\frac{\partial K_\perp}{\partial \xi} + \left(1-\frac{\eta f_\theta}{\xi}\right)^2 \frac{\partial K_\parallel}{\partial \xi}$$
$$+ 2\frac{\partial \eta}{\partial \xi}\left[\left(\eta f_\xi^2 + \frac{f_\theta}{\xi}+\eta\right)K_\perp - \left(1-\frac{\eta f_\theta}{\xi}\right)\frac{f_\theta}{\xi}K_\parallel\right]$$
$$+ 2\frac{f_\theta}{\xi^2}\left[-\left(\frac{f_\theta}{\xi}+\eta\right)K_\perp + \left(1-\frac{\eta f_\theta}{\xi}\right)\eta K_\parallel\right],$$

$$\frac{\partial D}{\partial \theta} = \left[(1+\eta^2)f_\xi^2 + \left(\frac{f_\theta}{\xi}+\eta\right)^2\right]\frac{\partial K_\perp}{\partial \theta} + \left(1-\frac{\eta f_\theta}{\xi}\right)^2 \frac{\partial K_\parallel}{\partial \theta}$$
$$+ 2\frac{\partial \eta}{\partial \theta}\left[\left(\eta f_\xi^2 + \frac{f_\theta}{\xi}+\eta\right)K_\perp - \left(1-\frac{\eta f_\theta}{\xi}\right)K_\parallel\right].$$

The plasma dielectric is given by the standard relations

$$K_\perp = 1 - \sum_{\sigma=i,e}\frac{\omega_{p\sigma}^2}{\omega^2-\omega_{c\sigma}^2}, \quad K_\parallel = 1 - \sum_{\sigma=i,e}\frac{\omega_{p\sigma}^2}{\omega^2},$$

where $\omega_{c\sigma}^2 = (q_0 B_z/m_\sigma c)^2(1+\eta^2)$ and $\omega_{p\sigma}^2 = 4n_\sigma q_0^2/m_\sigma$.

[1]R. K. Fisher and R. W. Gould, Phys. Rev. Lett. **22**, 1093 (1969); and Phys. Fluids **14**, 857 (1971).

[2]H. H. Kuehl, Phys. Fluids **16**, 1311 (1973).

[3]R. J. Briggs and R. R. Parker, Phys. Rev. Lett. **29**, 852 (1972).

[4]P. Bellan and M. Porkolab, Phys. Rev. Lett. **34**, 124 (1975); and Phys. Fluids **17**, 1592 (1974).

[5]S. Ejima, V. S. Chan, R. La Haye, C. Moeller, P. I. Petersen, and J. C. Wesley, Bull. Am. Phys. Soc. **22**, 1170 (1977).

[6]P. T. Bonoli and E. Ott, Phys. Fluids **25**, 359 (1982).

[7]M. Brambilla, Nucl. Fusion **16**, 47 (1976).

[8]P. M. Bellan, Phys. Rev. Lett. **45**, 1407 (1980).

[9]T. H. Stix, Phys. Rev. Lett. **15**, 878 (1965).

[10]P. M. Bellan and M. Porkolab, Phys. Fluids **19**, 995 (1976).

[11]P. M. Bellan and K. L. Wong, Phys. Fluids **21**, 592 (1978).

[12]R. L. Berger, L. Chen, P. K. Kaw, and F. W. Perkins, Phys. Fluids **20**, 1864 (1977).

[13]E. Ott, Phys. Fluids **22**, 1732 (1979).

[14]A. Sen and N. J. Fisch, Bull. Am. Phys. Soc. **23**, 789 (1978).

[15]R. E. Slusher, C. M. Surko, J. J. Schuss, R. R. Parker, I.H. Hutchinson, D. Overskei, and L. S. Scaturro, Phys. Fluids **25**, 457 (1982).

[16]B. Carreras, B. V. Waddell, and H. R. Hicks, Nucl. Fusion **19**, 1423 (1979).

[17]J. J. Schuss, M. Porkolab, Y. Takase, and S. Texter, Bull. Am. Phys. Soc. **26**, 1023 (1981).

[18]S. C. Luckhardt, M. Porkolab, S. F. Knowlton, K.-I. Chen, A. S. Fisher, F. S. McDermott, and M. Mayberry, Phys. Rev. Lett. **48**, 152 (1982).

[19]J. J. Schuss, S. Fairfax, B. Kusse, R. R. Parker, M. Porkolab, D. Gwinn, I. H. Hutchinson, D. Overskei, and L. Scaturro, Phys. Rev. Lett. **43**, 274 (1979).

[20]T. Yamamoto, T. Imai, M. Shimada, N. Suzuki, M. Maeno, S. Konoshima, T. Fujii, K. Uehara, T. Nagashima, A. Funahashi, and N. Fujisawa, Phys. Rev. Letters **45**, 716 (1980).

[21]S. Bernabei, R. Chrien, S. Davis, W. Hooke, D. Ignat, F. Jobes, R. Kaita, R. Motley, J. Stevens, and J. Strachan, Bull. Am. Phys. Soc. **26**, 975 (1981).

Downloaded 13 Dec 2007 to 131.215.225.196. Redistribution subject to AIP license or copyright; see http://pof.aip.org/pof/copyright.jsp